Biogeosciences Discuss., 9, 14945–14980, 2012
www.biogeosciences-discuss.net/9/14945/2012/
doi:10.5194/bgd-9-14945-2012

Biogeosciences Discussions

Spatial and temporal variability of N_2O emissions in a subtropical forest catchment in China

J. Zhu[1], J. Mulder[1], L. P. Wu[2], X. X. Meng[2], Y. H. Wang[3], and P. Dörsch[1]

[1]Norwegian University of Life Sciences, postbox 5003, Ås-1432, Norway
[2]Chongqing Academy of Environmental Sciences and Monitoring, Qishan Road 252, Chongqing, China
[3]Institute of Forest Ecology, Environment and Protection, Chinese Academy of Forestry, Wan-Shou-Shan, Beijing, 100091, China

Received: 19 September 2012 – Accepted: 9 October 2012 – Published: 29 October 2012

Correspondence to: J. Zhu (jing.zhu@umb.no)

Published by Copernicus Publications on behalf of the European Geosciences Union.

Abstract

Subtropical forests in South China have received chronically large amounts of atmogenic nitrogen (N) causing N saturation. Recent studies suggest that a significant proportion of the N input is returned to the atmosphere, in part as nitrous oxide (N_2O). We measured N_2O emission fluxes by closed chamber technique throughout two years in a Masson pine-dominated headwater catchment with acrisols (pH ~ 4) at TieShanPing (Chongqing, SW China) and assessed the spatial and temporal variability in two landscape elements typical for this region: a mesic forested hill slope (HS) and a hydrologically connected, terraced groundwater discharge zone (GDZ) in the valley bottom. High emission rates of up to 1800 µg N_2O-N m^{-2} h^{-1} were recorded on the HS shortly after rain storms during monsoonal summer, whereas emission fluxes during the dry winter season were generally low. Overall, N_2O emission was lower in GDZ than in HS, rendering the mesic HS the dominant source of N_2O in this landscape. Temporal variability of N_2O emissions on HS was largely explained by soil temperature and moisture, pointing at denitrification as a major process for N removal and N_2O production. The concentration of nitrate (NO_3^-) in pore water on HS was high even in the rainy season, apparently never limiting denitrification and N_2O production. The concentration of NO_3^- decreased along the terraced GDZ, indicating efficient N removal, but with moderate N_2O-N loss. The extrapolated annual N_2O fluxes from soils on HS (0.50 and 0.41 g N_2O-N m^{-2} yr^{-1} for a year with a wet and a dry summer, respectively) are among the highest N_2O fluxes reported from subtropical forests so far. Annual N_2O-N emissions amounted to 8–10 % of the annual atmogenic N-deposition, suggesting that forests on acid soils in South China are an important, hitherto overlooked component of the anthropogenic N_2O budget.

BGD
9, 14945–14980, 2012

1 Introduction

The global atmospheric concentration of nitrous oxide (N_2O), an important greenhouse gas and decomposer of stratospheric ozone, has increased from a pre-industrial level of 270 ppbv to 322 ppbv in 2008 (WMO, 2009). The global source strength is estimated to be 17.7 Tg N yr^{-1}, with agriculture contributing 2.8 (1.7–4.8) Tg N yr^{-1} and soils under natural vegetation 6.6 (3.3–9.0) Tg N yr^{-1} (IPCC, 2007; Hirsch et al., 2006). Both, estimates based on bottom-up approaches (Stehfest and Bouwman, 2006) and on observations of the N_2O atmospheric column (Kort et al., 2011; D'Amelio et al., 2009; Hirsch et al., 2006) suggest that 50–64 % of the atmospheric N_2O derive from the (sub)tropical zone 0° to 30° N. Much of the N_2O attributable to this zone is emitted from forest soils (Melillo et al., 2001; Werner et al., 2007a; Rowlings et al., 2012). So far, N_2O flux data from subtropical forests are scarce making this biome an under-investigated component of the global N_2O budget.

Large parts of southern China are situated in the humid subtropics and the dominant forest types are evergreen broadleaf and coniferous forest, many of which are found as patches in densely populated areas with intensive agriculture. Due to strong increases in the emission of nitrogen oxides (NO_x) and ammonia (NH_x), caused by combustion of fossil fuels and massive fertilizer use, respectively (Xiong et al., 2008; Liu et al., 2011b), these forests receive high amounts of reactive nitrogen (N_r) by atmogenic deposition, mostly as ammonium (NH_4^+). A recent study of five forested watersheds in South China found various degrees of N saturation (Chen and Mulder, 2007a), i.e. rates of atmogenic N_r input exceeding uptake by vegetation (Aber et al., 2003) and causing elevated concentrations of nitrate (NO_3^-) in the root zone. Larssen et al. (2011) reported moderate NO_3^- export with stream water in these watersheds, despite low forest productivity, suggesting major unaccounted N sinks in these ecosystems.

One possible fate of excess N may be gaseous emission as nitric oxide (NO), N_2O or dinitrogen (N_2) produced during nitrification and denitrification. Known factors controlling N_2O emissions are availability of inorganic N and degradable organic carbon

BGD
9, 14945–14980, 2012

(C), soil temperature, soil moisture and soil pH (Parton et al., 1996; Flessa et al., 1995; Smith et al., 2003; Weier et al., 1993; Simek and Cooper, 2002). The monsoonal climate in South China provides favorable conditions for both nitrification and denitrification as much of the annual N input, dominated by NH_4^+, occurs during rain storms in summer when soils are warm and N turnover rates high. Moreover, forests in South China are often found on acidic soils. Acidity has been reported to support high N_2O/N_2 ratios in denitrification (Liu et al., 2010; Bergaust et al., 2010), which could result in high N_2O emissions.

Few studies have addressed N_2O emissions in Chinese subtropical forests. Tang et al. (2006) studied the temporal variation of N_2O fluxes in a pine, a mixed and an evergreen broadleaf forest on acid soils in the Dinghushan catchment, South China throughout one year and found highest emissions during the hot-humid season. Based on weekly to biweekly measurements, they estimated an annual emission of 3.2 kg N_2O-N ha^{-1} which is above the reported average N_2O emission of 1.2–1.4 kg N ha^{-1} yr^{-1} for tropical forests (Stehfest and Bouwman, 2006; Werner et al., 2007b). Fang et al. (2009) reported 2.0 to 2.4 kg N_2O-N loss ha^{-1} yr^{-1} based on monthly measurements along a hillslope in an evergreen broadleaf forest in the same catchment. Lin et al. (2010, 2012) estimated smaller average annual N_2O emissions of 0.13 and 0.71 kg N ha^{-1} for pine forests in Hubei province, probably due to the higher pH of these forest soils.

Estimates of annual N_2O emissions in forested catchments are fraught by large temporal and spatial variability commonly reported for N_2O fluxes. Forests in subtropical China are typically found on sloping terrain and mountain ridges, resulting in hydrological gradients known to affect N_2O emissions. For example, Fang et al. (2009) found that N_2O emissions increased with soil moisture from hilltop to the bottom of a hill slope. Besides soil moisture, other soil factors, such as pH, texture, vegetation type and productivity may vary along hydrological flow paths, resulting in distinct spatial patterns of N_2O emissions (Osaka et al., 2006; Lark et al., 2004). Ultimately, soil factors related to topography may shape distinct nitrifier and denitrifier communities with respect to

BGD
9, 14945–14980, 2012

N_2O turnover (Philippot et al., 2009; Dörsch et al., 2012; Wessen et al., 2011; Banerjee and Siciliano, 2012). Thus, understanding of spatial and temporal variability of N_2O emission fluxes and their drivers on a landscape level are indispensable for improving regional estimates of N_2O emissions.

The objective of the present study was to estimate N_2O fluxes in an N-saturated forested catchment in Southwest China and to explore their main drivers in space and time. More specifically, we investigated the seasonal distribution of emission fluxes (dry versus wet season), the role of storm flow conditions for peak N_2O emissions and the spatial distribution of N_2O emissions along a hydrological flow path on a hill slope (HS) and a groundwater discharge zone (GDZ). We hypothesized the emission strength to be higher in the water-saturated GDZ than on the well-drained HS. To improve flux estimates, a regression model is proposed interpolating temporally discrete N_2O measurements on the HS based on continuously recorded soil moisture and temperature.

2 Materials and methods

2.1 Site description

The TSP catchment is a 16.2 ha headwater catchment, 450 m a.s.l., located on a forested ridge about 25 km Northeast of Chongqing city, SW China (29°38′ N 104°41′ E, Fig. 1a). Details on climate, vegetation, and soil characteristics as well as atmogenic N deposition can be found elsewhere (Chen and Mulder, 2007b). The area has a typical subtropical monsoonal climate with a mean annual precipitation of 1028 mm and a mean annual temperature of 18.2 °C (three year average, 2001–2003). 75 % of the rainfall occurs during summer (April to September). Mean annual inorganic N deposition (from 2001–2003) was 4 g m^{-2}, 61 % of which occurred in the form of NH_4^+-N (Chen and Mulder, 2007b). Data for more recent years show increasing N deposition rates to >5 g m^{-2} yr^{-1} and confirm the relative importance of NH_4^+ (L. Duan, personal communication, 2011). The vegetation is a coniferous-broadleaf mixed forest dominated

BGD
9, 14945–14980, 2012

by Masson pine (*Pinus massoniana*) with a well-developed understory of evergreen shrubs. Land use is a naturally regenerated, non-managed secondary forest after the original forest was cut down during 1958–1962.

For the present study, a representative 4.6 ha sub-catchment was selected, consisting of a NE facing hill slope (HS) and a hydrologically connected SE-NW oriented, terraced valley bottom acting as a ground water discharge zone (GDZ) (Fig. 1b). The HS is dominated by acidic, loamy yellow mountain soils (Haplic Acrisols; WRB, 2006), developed from sandstone, the predominant bedrock in the area. The turnover rate of soil organic matter (SOM) is high given the warm and wet climate (Raich and Schlesinger, 1992; Zhou et al., 2008), allowing little organic matter to accumulate (O horizon; 0–2 cm) (Table 1). Soils in the GDZ have developed from colluvium (Cambisols) and were terraced during the 1960s for vegetable cultivation but abandoned shortly after. The soils in the GDZ have a low hydraulic conductivity (Sørbotten, 2011), lack horizontal differentiation (no distinct O horizon) and have high ground water levels. The vegetation in the GDZ consists of sparse shrubs and grasses while trees taller than 2 m are absent. Clay mineralogy on HS and in GDZ is dominated by kaolinite. A recent study showed that considerable interflow occurs along HS during rainfall episodes. Excess water moves laterally in the surface horizons down slope over the argic B horizon, which has a low hydrological conductivity, draining the O/A and AB horizons on HS relatively quickly. Discharge of interflow into GDZ results in high ground water levels and periodic water-logging during summer (Sørbotten, 2011). Major soil characteristics for both locations are summarized in Table 1.

2.2 N_2O flux measurements

N_2O emissions were measured manually by closed chamber technique along two transects in the sub-catchment. Transect T was established perpendicular to the contour lines on the HS stretching from the hill top close to the watershed divide to the hill bottom close to the GDZ. Transect B was established in the GDZ following an elevation gradient of six hydrologically connected terraces (Fig. 1b) towards a flume, which

BGD
9, 14945–14980, 2012

was used to measure surface runoff from the subcatchment. Permanent micro-plots for N_2O emission measurements were established in triplicate at six plots along the T transect on HS (T1 to T5 and B1) and at five plots along the B transect in GDZ (B2 to B6; Fig. 1b) with plot B1 representing the transition between HS and GDZ. Two sampling strategies were applied to explore N_2O fluxes. A first measurement campaign during summer 2009 (July to September) with frequent flux measurements explored N_2O emission dynamics in response to sudden increase in soil moisture after rainfall episodes. A more regular sampling scheme with biweekly measurements was applied throughout the dry-cool season (November 2009 to March 2010) and during the subsequent summer (from April to August 2010), interrupted by more intensive measurement campaigns after individual rain storms (> 20 mm). For logistic reasons, only a selection of plots (T1, T3, T5, B1, B2, B4 and B6) was monitored during the dry season.

For flux sampling, closed zinc-coated iron chambers (30 cm diameter and 30 cm in height) were inserted approximately 2 cm into the loamy soil while keeping the air pressure constant via a vent tube attached to the top of the chamber (Hutchinson and Mosier, 1981). Four gas samples were taken from a sampling port 1, 5, 15 and 30 min after chamber deployment by a 20-ml plastic syringe. Samples were transferred immediately to pre-evacuated 12 ml-vials crimp sealed with butyl septa (Chromacol, UK), resulting in an overpressure to avoid contamination during shipment. Chamber temperature was recorded by inserting a handheld digital thermometer into the sampling port at beginning and end of chamber deployment. Gas samples were shipped to the Norwegian University of Life Sciences for analysis by ECD-gas chromatography (Model 7890A, Agilent, Santa Clara, CA, US). Carbon dioxide (CO_2) and N_2O were separated on a 20 m wide-bore (0.53 mm diameter) Poraplot Q column run at 38 °C after passing a packed Heysept column used for back-flushing water. Helium (He 5.0) was used as carrier gas. The ECD was run at 375 °C with 17 ml min^{-1} Ar/CH_4 (90/10 vol %) as make-up gas. N_2O emission rates ($\mu g\,N\,m^{-2}\,h^{-1}$) were calculated based on the rate of change in N_2O concentration in the chamber, which was estimated from the slope of a linear or a second order polynomial fit of the concentration data against time, the

BGD
9, 14945–14980, 2012

internal volume of the chamber, the covered soil surface area and the average chamber temperature during deployment. Cumulative N_2O emissions for observation periods in summer 2009 (27 days, 12 July to 8 August) and summer 2010 (106 days, 10 May to 24 August) were calculated assuming a constant flux rate between sampling dates.

2.3 Soil sampling and analysis

Soil samples were taken on 15 October 2009 from the eleven plots used for N_2O flux measurements, and analyzed for pH, total organic carbon (TOC) and total nitrogen (TN). Samples at plots T1 to T5 and B1 were taken from the O- (0–2 cm), A- (2–8 cm), AB- (8–20 cm) and B- (20–40 cm) horizons. In GDZ (plots B2 to B6), where an organic horizon was absent, the homogeneous 0–20 cm and 20–40 layers were sampled. Denitrification characteristics of the soils, investigated in a laboratory study, are reported elsewhere (Zhu et al., 2012). Briefly, the instantaneous denitrification rate (IDR; expressed in nmol N_2O-N g^{-1} dw soil h^{-1}) in soils from the different plots was estimated from the N_2O accumulation rate in acetylene-treated, anoxic soil slurries at 20 °C in the presence of ample NO_3^--N (2 mM). The soils' ex situ potential for N_2O loss (in nmol NO_3^--N g^{-1} dw soil) was estimated as the amount of NO_3^--N respired to N_2O before N_2O reductase was fully expressed and rapid N_2O reduction to N_2 occurred. This amount was generally < 10 % of the added NO_3^--N but varied with landscape position from which the soil samples were taken (Zhu et al., 2012). IDR declined rapidly below the A horizon (Table 1), indicating low denitrification activity in the deeper horizons. Therefore only data from the O and A horizons of HS and the 0–20 cm layer of GDZ are presented here.

Soil pH (H_2O) was measured in a suspension of 10 g dry weight (dw) soil in 50 ml de-ionized water with an Orion SA720 pH-meter connected to an Orion ROSS Ultra pH Electrode. The contents of TOC and TN in the soil were measured in the fine earth fraction (< 2 mm), obtained after drying at 105 °C and sieving, using an element analyser (Vario EL III, Elementar Analysensysteme GmbH, Germany) at the Research Center

BGD
9, 14945–14980, 2012

of Eco-environmental Science, Chinese Academy of Science (RCEES, CAS). In addition, soil samples from the horizons and layers of all plots were collected three times (15 October 2009, 22 January 2012 and 29 April 2010) to measure KCl-extractable nitrate ($NO_{3\ ex}^-$) and ammonium ($NH_{4\ ex}^+$). Soil samples were extracted by shaking 10 g dw equivalents of fresh soil with 50 ml of 2 M KCl for 1 h. The concentrations of NO_3^- and NH_4^+ in the filtered extract were determined using FIA (San^{++}, Skalar, the Netherlands) at RCEES, CAS.

Ceramic suction cup lysimeters (P80; Staatliche Porzellanmanufaktur, Berlin) and Macrorhizon soil moisture sampler (Rhizosphere Research Products, The Netherlands) were installed at each plot on HS and GDZ, respectively. On HS, lysimeters were installed in triplicate in the A- (4–5 cm), the top of the AB- (10 cm), the bottom of the AB- (20 cm) and in the B-horizon (40 cm). At GDZ, one Macrorhizon was installed at each of three depths (30, 60 and 100 cm). Soil water from HS was sampled from 11 November 2009, while groundwater was sampled from 5 August 2009; both were sampled at weekly intervals until spring 2010 and on each N_2O flux measurement date in summer 2010. Soil water from triplicate lysimeters per soil depth on HS was pooled prior to analysis. Concentrations of NO_3^- and NH_4^+ in lysimeter water were measured in each sample during wet-warm seasons and in pooled samples (four weeks) during the dry-cool season, using ion chromatography (DX-120 for NH_4^+ and DX-500 for NO_3^-, DIONEX, USA) at the Chongqing Academy of Environmental Sciences and Monitoring, China.

Soil bulk density (BD) of surface horizons/layers was measured from intact soil cores (100cc steel cylinders) sampled in triplicate at two depths (3.5–7.2 cm and 10–13.7 cm), corresponding to the A and AB horizons, respectively (Sørbotten, 2011).

Soil temperature (ST) and volumetric moisture (VM) at 10 cm depth were recorded every 10 min by TDR probes (Hydra Probe II) installed at plots T3 and B1 on 11 October 2009 and stored by a data logger (Campbell CR200). Soil water filled pore space (WFPS) was calculated using BD at depth of 10.0–13.7 cm, assuming a soil particle density (PD) of 2.65 g cm^{-3} as:

BGD
9, 14945–14980, 2012

$$\mathrm{WFPS}(\%) = \frac{\mathrm{VM}}{1 - \left(\frac{\mathrm{BD}}{\mathrm{PD}}\right)} \times 100 \quad (1)$$

Groundwater level (GWL) was monitored in PVC tubes, with a 30-cm nylon filter at the lower end, and installed at each plot along the B-transect in GDZ (B1 to B6). The PVC tubes were covered with a perforated lid to prevent pressure differences with the atmosphere. GWL was measured daily from Jul. 2009 to the beginning of August 2009 during a period of heavy rainstorms and on dates of N_2O measurements thereafter.

Meteorological data (air temperature (AT), precipitation (precip) and relative humidity (RH)) were obtained every 5 min from a weather station (WeatherHawk 232, USA), at the roof of the TSP Forest Bureau situated 1 km south of the catchment. Vapor pressure deficit (VPD) was calculated from Eq. (2) (ASCE, 2005) as:

$$\mathrm{VPD} = \left(\frac{\mathrm{RH}}{100} - 1\right) \times 0.6108 \times \exp(17.27 \times \mathrm{AT}(\mathrm{AT} + 237.3) \quad (2)$$

2.4 Statistical analysis

Cumulative N_2O emissions for each of 11 plots for summer 2010 (106 days) were analyzed together with soil parameters in the top soil (depth-weighted for O and O horizons on HS and from 0–20 cm in GDZ; Table 1) by Principal Component Analysis (PCA). Bulk density, cumulative N_2O flux, $NH_4^+{}_{sw}$ and $NO_3^-{}_{sw}$ were normalized using minus reciprocal, natural logarithmic, natural logarithmic and sinusoidal transformation, respectively.

To explore the seasonal drivers of the N_2O emission flux, log-transformed average N_2O emission rates on HS (average of 4 plots, T1, T3, T5 and B1, which had full N_2O flux datasets including the dry season) were subjected to stepwise multiple linear regression (MLR) with ST, WFPS (average of daily ST and WFPS obtained from TDR at both T3 and B1 from 12 October 2009 onwards), as well as pore water $NO_3^-{}_{sw}$ and $NH_4^+{}_{sw}$ as independent variables. The resulting empirical relation was used to

BGD
9, 14945–14980, 2012

interpolate the N_2O flux on HS between measurement dates and to estimate annual N_2O emission.

Missing values for ST and WFPS (from 1 May to 11 October 2009) were estimated on a daily basis, using a statistical model based on MLR, using meteorological parameters (average air temperature, rainfall and average VPD) and average ST and WFPS observed at plot T3 and B1 in the period 11 October 2009 to 24 December 2010.

Paired *t*-test was applied for the comparison of different plots and the two landscape elements. All statistical analyses were conducted with Minitab 16.1.1 (Minitab Inc.).

3 Results

3.1 Weather, soil moisture and soil temperature

Rainfall distribution during the wet season (April to October) differed between the two years (Fig. 2). Summer 2009 (1054 mm) was wetter than summer 2010 (850 mm) and precipitation occurred mostly as intensive rainstorms (up to 385 mm during 41 h between 3 and 5 August 2009). In contrast, precipitation was more evenly distributed in the summer 2010. Only 117 mm rain fell in the dry-cool season from November 2009 to March 2010. Soil WFPS at 10 cm depth on the mid slope (T3, mean WFPS 55.8 %) was significantly smaller than at the foot slope of HS at the transition to GDZ (B1, mean WFPS 70.0 %) (Fig. 3a), most likely reflecting convergence of interflow from HS at B1. In winter, WFPS was relatively stable with values around 56.7 % for T3 and 68.5 % for B1. In contrast, large variations in WFPS were observed in spring and summer, driven by precipitation, and subsequent drainage and evapotranspiration. In plot T3 (HS), but not in plot B1 (transition to GDZ), WFPS decreased significantly in late summer 2010 (July through September), indicating drier conditions on the upper part of HS as described earlier for this site (Mulder et al., 2005). Soil temperature at 10 cm depth varied seasonally between 10 °C and 25 °C with no significant difference between T3 and B1,

BGD
9, 14945–14980, 2012

although the drier T3 plot tended to have somewhat higher soil temperatures during the wet season (Fig. 3b).

The GWL in GDZ varied between +15 cm (above surface) and < −100 cm (below surface), with highest values at B5 and lowest at B1 (Fig. 4). The heavy rainstorm between 3 and 5 August 2009 resulted in a rapid increase of the GWL. The GWL reached its lowest values from late summer onwards, but increased in early spring, due to increased precipitation in March and April 2010. In general, GWL ranged in the order B 1> B2 = B3 = B4 > B5 > B6 and was most stable close to the outlet (plots B5 and B6), whereas GWL was only occasionally detectable (> −100 cm depth) at plots B1, B2 and B3 (Fig. 4).

3.2 N_2O fluxes

Emission fluxes of N_2O showed a pronounced seasonal pattern with highest values during summer (warm-humid season) and generally low emission rates during winter (dry-cool season) (Fig. 5). During summer, N_2O emission rates varied 2–3 orders of magnitude, with highest values immediately following precipitation events (compare Figs. 2 and 5) when WFPS was high (Fig. 3a). In summer 2010, with its more even distribution of rainfall, peak N_2O emissions were smaller (450 $\mu g\, m^{-2}\, h^{-1}$) than in summer 2009 (1730 $\mu g\, N\, m^{-2}\, h^{-1}$) (Fig. 5). Cumulative N_2O emissions in summer 2009 (27 days) and in summer 2010 (106 days) were greater on HS (including B1) than in GDZ (B2–B6) in both periods (Fig. 6). Averaged on a daily basis, N_2O fluxes on HS were higher in summer 2009 (6.4 mg N m^{-2} d^{-1}) than in summer 2010 (3.2 $mg\, N\, m^{-2}\, d^{-1}$). The average N_2O emissions were smaller in GDZ, emitting 3.2 $mg\, N_2O\text{-}N\, m^{-2}\, d^{-1}$ and 1.8 $mg\, N_2$ O-N $m^{-2}\, d^{-1}$ in 2009 and 2010, respectively. The spatial variability within the plots was high particularly on HS (Fig. 6) and no significant differences in cumulative N_2O emissions were found between plots within the same landscape element. The spatial pattern in cumulative N_2O flux for the plots within one transect was not consistent for the two summer periods (Fig. 6).

BGD
9, 14945–14980, 2012

3.3 Spatial variation in soil factors controlling N_2O emissions

Surface soil had a greater bulk density in GDZ than on HS (Table 1) even though there were exceptions (plots B4 and B5). The pH of the surface soil was significantly higher in GDZ than on HS (Table 1). For TOC, TN and C/N the opposite was the case, reflecting the lack of an organic surface layer in GDZ. Values for $NO_{3\ ex}^-$ and $NO_{3\ sw}^-$ were significantly higher on HS than in GDZ. In the O-horizon, TOC and TN were higher at T2 and T4 than at other plots on HS. Plot B6 was highest in GDZ with respect to these variables. The concentration of NO_3^- in soil water ($NO_{3\ sw}^-$) was high in winter and early spring and decreased sharply at the start of the growing season in early April, probably due to biological uptake of N and dilution by ample rainfall at the end of March 2010 (Fig. 7). During winter, $NO_{3\ sw}^-$ showed consistent differences among plots on HS with highest values at plot T1 and lowest at plot T2, whereas concentrations were lower and more uniform throughout summer, fluctuating with precipitation events. There were consistent differences in $NO_{3\ sw}^-$ in GDZ, with concentration levels decreasing in the order B2 = B4 > B3 > B5 > B6. At B3, B5 and B6, $NO_{3\ sw}^-$ concentrations were below 5 mg N l^{-1} during most of the year with the greatest values at the end of the dry season (February and March 2010). The concentration of NH_4^+ in soil water ($NH_{4\ sw}^+$) was small, with values amounting to less than 10 % of total inorganic N in solution, except for plots B2 and B6, and there was no seasonal pattern in any of the plots (data not shown). No correlation was found between $NH_{4\ sw}^+$ and $NO_{3\ sw}^-$ in soil water.

We used PCA to assess the relationship between soil parameters and the cumulative N_2O flux in summer 2010 (Fig. 8) at each plot (Fig. 6). The plots divided into two groups (T1 to T5 and B1 as one group (HS); the others as the second group (GDZ)). The first two components of PCA explained 63.9 % of the total variation in N_2O emission flux, with most of the physicochemical parameters (pH, bulk density, TOC, TN, $NO_{3\ ex}^-$, $NO_{3\ sw}^-$ and $NH_{4\ ex}^+$) and the ex situ potential for N_2O loss contributing to the first component (50.3 %). The second component (13.6 %) included $NH_{4\ sw}^+$. The initial denitrification rate (IDR) contributed to both components, but had relatively small effect

BGD
9, 14945–14980, 2012

on the N_2O flux compared to other parameters. Total organic carbon (TOC) and most of the variables associated with the availability of N (TN, $NO_{3\ ex}^-$, $NO_{3\ sw}^-$ and $NH_{4\ ex}^+$) were positively correlated with soil N_2O flux, whereas soil pH and BD were negatively correlated with N_2O flux. Also, IDR and the ex situ potential for N_2O loss were positively correlated with N_2O flux, whereas $NH_{4\ sw}^+$ concentration in soil water did not correlate with N_2O flux.

3.4 Temporal variation of seasonal drivers for N_2O emission

In summer, peak N_2O emission was associated with rainfall resulting in high WFPS values. Emission of N_2O on HS was highest at WFPS values between 63 % and 72 % (averages at 10 cm soil depth for T3 and B1, respectively) and appeared somewhat lower at values larger than 75 % (Figs. 3a and 5). Figure 5 illustrates the large inter-annual variation of N_2O flux between a wet year with intensive rainfall episodes (2009) and a relatively dry year (2010) with only one episode with precipitation $> 50\,mm\,day^{-1}$ (82 mm in 9 h on 5 July 2010). The N_2O flux on HS was weakly, but negatively correlated with $NO_{3\ sw}^-$ ($p = 0.064$) whereas no correlation was found with $NH_{4\ sw}^+$ ($p = 0.659$). At individual sites in GDZ, the N_2O flux was weakly, but negatively correlated with GWL, i.e. higher N_2O flux occurred when GWL was low. Low soil temperature (ST) together with low WFPS seemed to be the main constraints for N_2O emission activity in winter (Figs. 3 and 5). Stepwise multi-linear regression (MLR) indicated that ST and WFPS were the only significant variables explaining temporal variability of N_2O emissions (Eq. 3) on HS; $NO_{3\ sw}^-$ and $NH_{4\ sw}^+$ concentrations did not add significantly and were excluded by the MLR. The residuals of the simulated values were normally distributed (not shown), suggesting unbiased fitting of the equation:

$$\ln(N_2O_{HS}) = -4.80 + 0.0881\,WFPS + 0.178\,ST$$
$$R - S(adj) = 68.9\,\% \qquad (3)$$

Since no data for ST and WFPS before 11 October 2009 was available, we used MLR to derive an equation that links ST and WFPS to meteorological data. The resulting

BGD
9, 14945–14980, 2012

regression models, presented in Eqs. (4) and (5) were then used to estimate the missing values prior to 11 October 2009:

$$ST = 7.84 + 0.579\,AT + 1.20\,VPD$$
$$R - Sq(\text{adj}) = 67.4\,\% \quad (4)$$

$$WFPS = 63.2 + 0.209 precip_5 + 1.84\,VPD_5$$
$$R - Sq(\text{adj}) + = 58.8\,\% \quad (5)$$

where $precip_5$ is the day-weighted 5-day average precipitation prior to the date for which the computation was done (calculated as $1.0\times precip_{day(0)} + 0.8\times precip_{day(-1)} + 0.6\times precip_{day(-2)} + 0.4\times precip_{day(-3)} + 0.2\times precip_{day(-4)}$) and VPD_5 the day-weighted 5-day average vapor pressure deficit calculated analogously. The selected weights explained the observations best. The residuals of the model simulations were normally distributed (not shown). Eq. 3 was used to estimate N_2O emissions using measured and, for the period prior to 11 October 2009, simulated values for ST (Eq. 4) and WFPS (Eq. 5). Measured and simulated values are shown in Fig. 9.

3.5 Annual N_2O flux

Annual N_2O emissions on the HS were calculated on a daily time step from equation 3 for two 1-yr periods (May 2009–April 2010 and January 2010 to December 2010), both years sharing the same winter period (Fig. 5), when N_2O emissions were small. The first annual period represents a relatively wet summer, whereas the second period a relatively dry summer. Annual N_2O fluxes for HS were 0.50 and 0.41 g N m^{-2} for the two years, respectively. The N_2O emission occurring during the first 5 days after the largest rainfall episode (4 to 5 August 2009) contributed 15.8 % to the annual N_2O emission of the first period. Emissions during the cool-dry season (November 2009 to March 2010) contributed 11.5 % to the annual flux of N_2O.

BGD
9, 14945–14980, 2012

4 Discussion

N_2O emission rates recorded after the heavy rainstorm in 2009 (up to 1730 µg N_2O-N m^{-2} h^{-1}; Fig. 5) are the highest found for forest ecosystems so far and exceed rates reported for (sub)tropical forests which typically vary between 11 to 600 µg N_2O-N m^{-2} h^{-1} (Liu et al., 2011a; Zhang et al., 2008; Silver et al., 2005; Ishizuka et al., 2005; Koehler et al., 2009; Rowlings et al., 2012; Kiese and Butterbach-Bahl, 2002).

Temporal variability (Fig. 5) exceeded spatial variability in both landscape elements (HS and GDZ). However, small-scale (within-plot) variability of the cumulated N_2O flux over the active season was high as seen from the high standard errors in Fig. 6 (particularly for HS). Probably this small scale variability was blurring existing trends in flux strength between plots along HS. High small-scale spatial variability of N_2O emissions is often reported for forests soils (Robertson and Klemedtsson, 1996; Bowden et al., 1992; Werner et al., 2007b) and commonly attributed to small-scale variation in mineral N availability, litter quality and soil moisture. We arranged the plots along transects perpendicular to the contour lines in the two landscape units as we expected that gradients in WFPS on HS and in GWL in GDZ would affect N_2O emissions by controlling aeration, substrate level and ultimately microbial activity (Garten et al., 1994). However, we did not find any consistent relationship between cumulative N_2O emission and plot position in neither of the two landscape elements. Concentrations of $NO_{3\ sw}^-$ on HS were similar at all plots during the warm-wet season (Fig. 7a) and did not correlate with N_2O emissions. NO_3^- availability was higher than in other studies (e.g., Koehler et al., 2009; Zhang et al., 2008) and appeared to be none-limiting for N_2O production on the HS, probably explaining the lack of a directional gradient in cumulative N_2O emissions as reported by others (Nishina et al., 2009; Fang et al., 2009). Surprisingly, the clear difference in WFPS between the mid slope position T3 and the foot slope position B1 (Fig. 3a) in spring and early summer did not result in significantly different cumulative N_2O emissions in neither year (Fig. 6). This was probably due to the fact

BGD
9, 14945–14980, 2012

that soil moisture was measured at 10 cm depth (in the upper AB-horizon), rather than in the zone of maximum denitrification activity, located in the uppermost soil layers (O and A horizons; Zhu et al., 2012). Soil moisture data records for 5 cm depth were incomplete due to sensor problems, but comparing existing data and bulk densities at 5 cm depth suggests that WFPS was more similar in the uppermost soil layer (data not shown). The pronounced decrease in WFPS at T3 (but not B1), later in summer, markedly reduced N_2O emissions as compared with B1 (insert Fig. 5). Together, this indicates that hydrology on HS had some impact on N_2O emission rates most probably through controlling denitrification.

In GDZ, decreasing NO_3^- concentrations along the hydrological flow path (Fig. 7b) suggested strong N retention; however, no correlation was found between cumulative N_2O emissions and average $NO_{3\ sw}^-$ at GDZ plots. There was a weak trend of decreasing cumulative N_2O emissions with increasing average GWL along the hydrological flow path in the GDZ (with the exception of B3) during summer 2009, when GWL was very dynamic (Fig. 6a). No such pattern was seen in the hydrologically more stable summer of 2010 (Fig. 6b). In general, GWL fluctuations are likely to interact with NO_3^- in controlling N_2O emissions, as rise of GWL can transport NO_3^- into C-richer upper soil layers and create anoxia favorable for denitrification. At the same time, the residence time of N_2O in the soil profile increases, due to decreasing diffusion, promoting reduction of N_2O to N_2. Conversely, a drop in GWL may relief gaseous diffusion constraints leading to release of N_2O from the soil. In summer 2010 (insert in Fig. 5), for instance, N_2O emission rates were lowest at B6 until GWL dropped about 10 cm in the middle of July (Fig. 4), resulting in a single N_2O emission peak while returning to low levels quickly thereafter. Similar N_2O dynamics have been observed in rice paddies (e.g. Qin et al., 2010). We found a positive correlation between dissolved N_2O (data not shown) and $NO_{3\ sw}^-$ in groundwater in both summers, indicating that N_2O production is overall NO_3^- limited in GDZ and likely coupled to N removal.

We found clear differences in N_2O source strength and environmental controls when comparing HS and GDZ; average cumulative N_2O emission in GDZ was roughly half

BGD
9, 14945–14980, 2012

of this at HS in both summers (Figs. 5 and 6), which was surprising, as we expected GDZ to behave as a riparian zone with elevated denitrification activity. Riparian zones are commonly considered as "hot spots" for N_2O emissions, because they receive dissolved N (DON, NO_3^-) from surrounding slopes while providing optimal conditions for denitrification (DOC, anoxia) (Groffman et al., 2000; Hefting et al., 2003). However, unlike common riparian zones which typically develop soils rich in organic matter, the GDZ studied here is formed by formerly cultivated terraces on colluvial deposits. Soils are dense and have low hydrological conductivities, resulting in low productivity and low TOC contents (Table 1). Laboratory incubations revealed that the GDZ soils had instantaneous denitrification rates (IDR) similar to HS soils, despite their markedly lower TOC contents (Zhu et al., 2012). This indicated a similar N removal potential in GDZ as compared with HS. However in their study, Zhu et al. (2012) also found that denitrifying communities on HS and in GDZ differed functionally with respect to their product stoichiometry, with the GDZ communities being more efficient in reducing NO_3^- all the way to N_2. Thus, the lower N_2O/N_2 ratio, and consequently the reduced N_2O emission rate, in GDZ may be attributed to a number of site-specific factors, directly or indirectly affecting denitrifier functioning and stoichiometry: (1) pore water at GDZ had lower NO_3^- concentrations (Figs. 7b and 8) which may decrease the N_2O/N_2 ratio by forcing denitrifiers to utilize N_2O as an additional electron acceptor, (2) diffusion of N_2O in soil is slow in dense GDZ soils, resulting in higher dissolved N_2O concentrations in pore water (data not shown) which support denitrifier communities to express N_2O reductase and (3) soil pH at GDZ was 0.5–0.6 units higher than at HS, which directly (Bergaust et al., 2010) or indirectly (Liu et al., 2010; Simek and Cooper, 2002; Dörsch et al., 2012) lowers N_2O/N_2 ratios.

Even though the N_2O emission flux was differently regulated in the two landscape elements, denitrification controls seemed to prevail over nitrification controls during the active periods. This is in agreement with the N_2O stoichiometry of the two processes; the N_2O/NO_3^- ratio of nitrification is generally $< \sim 1\,\%$ in moderately acid soils but may be higher in strongly acid soils, due to chemodenitrification of NO_2^- (Mørkved et al.,

BGD
9, 14945–14980, 2012

2007). Nitrification rates in the acidic forest soils of SW China are low (Cai and Zhao, 2009) and unlikely to be high enough to support the magnitude of N_2O emissions rates observed in both summers. We conducted an in situ $^{15}NO_3^-$ labeling experiment in summer 2010 at two positions along the HS to be reported elsewhere (Zhu et al., 2012) and found that 70–100 % of the emitted N_2O derived from the labeled soil NO_3^- pool. Denitrification as the predominant process for N removal and N_2O production on HS is further supported by the finding that N_2O concentrations measured in soil air were negatively correlated with pO_2 ($R^2 = 0.40$, $p < 0.05$, data not shown).

We found large temporal variability in N_2O fluxes. MLR identified soil temperature and moisture as the main drivers, explaining 68.9 % of the temporal variability of N_2O emission fluxes on HS. Such high coefficient of determination with only two variables (soil temperature and WFPS) is remarkable as most studies conducted in forest ecosystems find much lower degree of explanation by ancillary variables (Morishita et al., 2011; Gu et al., 2011). As shown in Fig. 9, the resulting regression model captured reasonably well both the seasonal distribution of emission fluxes and the transient emission peaks after rainfall events on HS except for the first measurement point. Peak N_2O emissions (Fig. 5) were triggered by spikes in WFPS (Fig. 3a) occurring after big rain episodes, resulting in a highly skewed distribution of N_2O fluxes as found in many other studies (Khalil et al., 2007; Venterea et al., 2009). Low soil temperature, together with relatively low WFPS throughout winter resulted in low N_2O fluxes. This implies that N_2O emission flux can be estimated fairly well from discontinuous flux measurements when continuous data on soil temperature and WFPS are available. However, it is important to sample fluxes closely around major rain fall events in summer as they contribute disproportionally to overall emissions. Too long interval between samplings may result in over- or under-estimation of the cumulative flux (Parkin, 2008).

Annual N_2O emissions for the TSP catchment were estimated for the HS only, since 96.4 % of the area consists of hill slopes, rendering GDZ emissions a minor component of the overall N_2O budget. Annual fluxes showed considerable variation between the wet year 2009 with several intensive rain episodes (0.50 g N_2O-N m^{-2} yr^{-1}) and the

BGD
9, 14945–14980, 2012

dryer year 2010 with more evenly distributed precipitation (0.41 g N_2O-N m^{-2} yr^{-1}). The average annual N_2O emission flux in TSP (0.45 g N m^{-2} yr^{-1}) is at the high end of annual N_2O emission fluxes (0.005–0.47 g N m^{-2} yr^{-1}) reported for unfertilized forestland in China (Cai, 2012) and even comparable to the high end of reported N_2O fluxes in tropical rainforests where temperatures are high throughout the year (Dalal and Allen, 2008). Expressed as a fraction of the annual atmogenic N-deposition, N_2O-N emission amounted between 8 and 10 % of the incoming inorganic N. This "emission factor" is remarkably high when compared to the IPCC Tier 1 factor for cultivated land (1 %) and pinpoints the prominent role of acid subtropical forests as a secondary source of anthropogenic N_2O which should be taken into account for regional N_2O budgets.

Acknowledgements. This study was supported by the Norwegian research council (Nordklima program 193725/S30: "N_2O emissions from N saturated subtropical forest in South China") and the Chinese Academy of Sciences (No. KZCX2-YW-GJ01 and GJHZ1205). We are grateful for technical support by Zhang Guanli at the Chongqing Academy of Environmental Sciences, Zhang Xiaoshan at the Research Center for Eco-environmental Sciences, Chinese Academy of Sciences and T. Fredriksen at the Norwegian University of Life Sciences. We also thank Duan Lei at the Tsinghua University for providing N deposition data and L. E. Sørbotten and J. Stolte (both Norwegian Institute for Agricultural and Environmental Research, Norway) for data on soil hydrology and assistance in the field.

References

Aber, J. D., Goodale, C. L., Ollinger, S. V., Smith, M. L., Magill, A. H., Martin, M. E., Hallett, R. A., and Stoddard, J. L.: Is nitrogen deposition altering the nitrogen status of northeastern forests? Bioscience, 53, 375–389, 2003.

ASCE: The ASCE standardized reference evapotranspiration equation, Environmental and Water Resources Institute of the American Society of Civil Engineers, 2005.

Banerjee, S. and Siciliano, S. D.: Factors driving potential ammonia oxidation in Canadian arctic ecosystems: does spatial scale matter? Appl. Environ. Microbiol., 78, 346–353, 2012.

BGD
9, 14945–14980, 2012

Bergaust, L., Mao, Y. J., Bakken, L. R., and Frostegård, A.: Denitrification response patterns during the transition to anoxic respiration and posttranscriptional effects of suboptimal pH on nitrogen oxide reductase in *Paracoccus denitrificans*, Appl. Environ. Microbiol., 76, 6387–6396, 2010.

Bowden, W. B., Mcdowell, W. H., Asbury, C. E., and Finley, A. M.: Riparian nitrogen dynamics in 2 geomorphologically distinct tropical rain-forest watersheds – nitrous-oxide fluxes, Biogeochemistry, 18, 77–99, 1992.

Cai, Z. C. and Zhao, W.: Effects of land use types on nitrification in humid subtropical soils of China, Acta Pedologica Sinica, 46, 7, 2009 (in Chinese).

Cai, Z. C.: Greenhouse gas budget for terrestrial ecosystems in China, Sci. China-Earth Sci., 55, 173–182, 2012.

Chen, X. Y. and Mulder, J.: Indicators for nitrogen status and leaching in subtropical forest ecosystems, South China, Biogeochemistry, 82, 165–180, 2007a.

Chen, X. Y. and Mulder, J.: Atmospheric deposition of nitrogen at five subtropical forested sites in South China, Sci. Total Environ., 378, 317–330, 2007b.

Dalal, R. C. and Allen, D. E.: Greenhouse gas fluxes from natural ecosystems, Aust. J. Bot., 56, 369–407, 2008.

D'Amelio, M. T. S., Gatti, L. V., Miller, J. B., and Tans, P.: Regional N_2O fluxes in Amazonia derived from aircraft vertical profiles, Atmos. Chem. Phys., 9, 8785–8797, doi:10.5194/acp-9-8785-2009, 2009.

Dörsch, P., Braker, G., and Bakken, L. R.: Community specific pH response of denitrification: experiments with cells extracted from organic soils, FEMS Microbiol. Ecol., 79, 530–541, 2012.

Fang, Y. T., Gundersen, P., Zhang, W., Zhou, G. Y., Christiansen, J. R., Mo, J. M., Dong, S. F., and Zhang, T.: Soil-atmosphere exchange of N_2O, CO_2 and CH_4 along a slope of an evergreen broad-leaved forest in southern China, Plant Soil, 319, 37–48, 2009.

Flessa, H., Dörsch, P., and Beese, F.: Seasonal-variation of N_2O and CH_4 fluxes in differently managed arable soils in southern Germany, J. Geophys. Res.-Atmos., 100, 23115–23124, 1995.

Garten, C. T., Huston, M. A., and Thoms, C. A.: Topgraphic variation of soil-nitrogen dynamics at Walker Branch watershed, Tennessee, Forest. Sci., 40, 497–512, 1994.

BGD
9, 14945–14980, 2012

Groffman, P. M., Gold, A. J., and Addy, K.: Nitrous oxide production in riparian zones and its importance to national emission inventories, Chemosphere – Global Change Science, 2, 291–299, 2000.

Gu, J. X., Nicoullaud, B., Rochette, P., Pennock, D. J., Henault, C., Cellier, P., and Richard, G.: Effect of topography on nitrous oxide emissions from winter wheat fields in Central France, Environ. Pollut., 159, 3149–3155, 2011.

Hefting, M. M., Bobbink, R., and de Caluwe, H.: Nitrous oxide emission and denitrification in chronically nitrate-loaded riparian buffer zones, J. Environ. Qual., 32, 1194–1203, 2003.

Hirsch, A. I., Michalak, A. M., Bruhwiler, L. M., Peters, W., Dlugokencky, E. J., and Tans, P. P.: Inverse modeling estimates of the global nitrous oxide surface flux from 1998–2001, Global Biogeochem. Cy., 20, GB1008, doi:10.1029/2004GB002443, 2006.

Hutchinson, G. L. and Mosier, A. R.: Improved soil cover method for field measurement of nitrous oxide fluxes, Soil Sci. Soc. Am. J., 45, 311–316, 1981.

IPCC (2007) Summary for policy makers, in: Climate Change 2007: The Physical Science Basis. Contribution of Working Group I to the Fourth Assessment Report of the Intergovernmental Panel on Climate Change, edited by: Solomon, S., Qin, D., Manning, M., Chen, Z., Marquis, M., Averyt, K. B., Tignor, M., and Miller, H. L., Cambridge, UK and New York, USA, 2007.

Ishizuka, S., Iswandi, A., Nakajima, Y., Yonemura, L., Sudo, S., Tsuruta, H., and Muriyarso, D.: Spatial patterns of greenhouse gas emission in a tropical rainforest in Indonesia, Nutr. Cycl. in Agroecosys., 71, 55–62, 2005.

Khalil, M. I., Van Cleemput, O., Rosenani, A. B., and Schmidhalter, U.: Daytime, temporal, and seasonal variations of N_2O emissions in an upland cropping system of the humid tropics, Commun. Soil Sci. Plan., 38, 189–204, 2007.

Kiese, R. and Butterbach-Bahl, K.: N_2O and CO_2 emissions from three different tropical forest sites in the wet tropics of Queensland, Australia, Soil Biol. Biochem., 34, 975–987, 2002.

Koehler, B., Corre, M. D., Veldkamp, E., Wullaert, H., and Wright, S. J.: Immediate and long-term nitrogen oxide emissions from tropical forest soils exposed to elevated nitrogen input, Glob. Change Biol., 15, 2049–2066, 2009.

Kort, E. A., Patra, P. K., Ishijima, K., Daube, B. C., Jimenez, R., Elkins, J., Hurst, D., Moore, F. L., Sweeney, C., and Wofsy, S. C.: Tropospheric distribution and variability of N_2O: Evidence for strong tropical emissions, Geophys. Res. Lett., 38, L15806, doi:10.1029/2011GL047612, 2011.

BGD
9, 14945–14980, 2012

Lark, R. M., Milne, A. E., Addiscott, T. M., Goulding, K. W. T., Webster, C. P., and O'Flaherty, S.: Scale- and location-dependent correlation of nitrous oxide emissions with soil properties: an analysis using wavelets, Eur. J. Soil Sci., 55, 611–627, 2004.

Larssen, T., Duan, L., and Muder, J.: Deposition and leaching of sulfur, nitrogen and calcium in four forested catchments in China: implications for acidification, Environ. Sci. Technol., 45, 1192–1198, 2011.

Lin, S., Iqbal, J., Hu, R. G., and Feng, M. L.: N_2O emissions from different land uses in mid-subtropical China, Agric. Ecosyst. Environ., 136, 40–48, 2010.

Lin, S., Iqbal, J., Hu, R. G., Ruan, L. L., Wu, J. S., Zhao, J. S., and Wang, P. J.: Differences in nitrous oxide fluxes from red soil under different land uses in mid-subtropical China, Agric. Ecosyst. Environ., 146, 168–178, 2012.

Liu, B. B., Mørkved, P. T., Frostegård, A., and Bakken, L. R.: Denitrification gene pools, transcription and kinetics of NO, N_2O and N_2 production as affected by soil pH, FEMS Microbiol. Ecol., 72, 407–417, 2010.

Liu, J., Jiang, P. K., Li, Y. F., Zhou, G. M., Wu, J. S., and Yang, F.: Responses of N_2O Flux from Forest Soils to Land Use Change in Subtropical China, Bot. Rev., 77, 320–325, 2011a.

Liu, X. J., Duan, L., Mo, J. M., Du, E. Z., Shen, J. L., Lu, X. K., Zhang, Y., Zhou, X. B., He, C. N., and Zhang, F. S.: Nitrogen deposition and its ecological impact in China: An overview, Environ. Pollut., 159, 2251–2264, 2011b.

Melillo, J. M., Steudler, P. A., Feigl, B. J., Neill, C., Garcia, D., Piccolo, M. C., Cerri, C. C., and Tian, H.: Nitrous oxide emissions from forests and pastures of various ages in the Brazilian Amazon, J. Geophys. Res.-Atmos., 106, 34179–34188, 2001.

Morishita, T., Aizawa, S., Yoshinaga, S., and Kaneko, S.: Seasonal change in N_2O flux from forest soils in a forest catchment in Japan, J. For. Res., 16, 386–393, 2011.

Mørkved, P. T., Dörsch, P., and Bakken, L. R.: The N_2O product ratio of nitrification and its dependence on long-term changes in soil pH, Soil Biol. Biochem., 39, 2048–2057, 2007.

Mulder, J., Chen, X. Y., Zhao, D. W., and Xiang, R. J.: Elevated nitrogen deposition in subtropical Chinese forest ecosystems, dominated by Masson pine: Nitrogen fluxes and budgets at the plot and catchment scale, The 3rd international N conference, Nanjing, China, 12–16 October 2004, 2005.

Nishina, K., Takenaka, C., and Ishizuka, S.: Spatiotemporal variation in N_2O flux within a slope in a Japanese cedar (Cryptomeria japonica) forest, Biogeochemistry, 96, 163–175, 2009.

BGD
9, 14945–14980, 2012

Osaka, K., Ohte, N., Koba, K., Katsuyama, M., and Nakajima, T.: Hydrologic controls on nitrous oxide production and consumption in a forested headwater catchment in central Japan, J. Geophys. Res.-Biogeosci., 111, 11, G01013, doi:10.1029/2005JG000026, 2006.

Parkin, T. B.: Effect of sampling frequency on estimates of cumulative nitrous oxide emissions, J. Environ. Qual., 37, 1390–1395, 2008.

Parton, W. J., Mosier, A. R., Ojima, D. S., Valentine, D. W., Schimel, D. S., Weier, K., and Kulmala, A. E.: Generalized model for N_2 and N_2O production from nitrification and denitrification, Global Biogeochem. Cy., 10, 401–412, 1996.

Philippot, L., Cuhel, J., Saby, N. P. A., Cheneby, D., Chronakova, A., Bru, D., Arrouays, D., Martin-Laurent, F., and Simek, M.: Mapping field-scale spatial patterns of size and activity of the denitrifier community, Environ. Microbiol., 11, 1518–1526, 2009.

Qin, Y. M., Liu, S. W., Guo, Y. Q., Liu, Q. H., and Zou, J. W.: Methane and nitrous oxide emissions from organic and conventional rice cropping systems in Southeast China, Biol. Fert. Soils, 46, 825–834, 2010.

Raich, J. W. and Schlesinger, W. H.: The global carbon dioxide flux in soil respiration and its relationship to vegetation and climate, Tellus B, 44, 81–99, 1992.

Robertson, K. and Klemedtsson, L.: Assessment of denitrification in organogenic forest soil by regulating factors, Plant Soil, 178, 49–57, 1996.

Rowlings, D. W., Grace, P. R., Kiese, R., and Weier, K. L.: Environmental factors controlling temporal and spatial variability in the soil-atmosphere exchange of CO_2, CH_4 and N_2O from an Australian subtropical rainforest, Glob. Change Biol., 18, 726–738, 2012.

Sørbotten, L.: Hill slope unsaturated flowpaths and soil moisture variability in a forested catchment in southwest China, Master thesis, Department of Plant and Environmental Sciences, Norwegian University of Life Sciences, Aas, 64 pp., 2011.

Silver, W. L., Thompson, A. W., McGroddy, M. E., Varner, R. K., Dias, J. D., Silva, H., Crill, P. M., and Keller, M.: Fine root dynamics and trace gas fluxes in two lowland tropical forest soils, Glob. Change Biol., 11, 290–306, 2005.

Simek, M. and Cooper, J. E.: The influence of soil pH on denitrification: progress towards the understanding of this interaction over the last 50 years, Eur. J. Soil Sci., 53, 345–354, 2002.

Smith, K. A., Ball, T., Conen, F., Dobbie, K. E., Massheder, J., and Rey, A.: Exchange of greenhouse gases between soil and atmosphere: interactions of soil physical factors and biological processes, Eur. J. Soil Sci., 54, 779–791, 2003.

BGD
9, 14945–14980, 2012

Stehfest, E. and Bouwman, L.: N_2O and NO emission from agricultural fields and soils under natural vegetation: summarizing available measurement data and modeling of global annual emissions, Nutr. Cycl. Agroecosys., 74, 207–228, 2006.
Tang, X. L., Liu, S. G., Zhou, G. Y., Zhang, D. Q., and Zhou, C. Y.: Soil-atmospheric exchange of CO_2, CH_4, and N_2O in three subtropical forest ecosystems in southern China, Glob. Change Biol., 12, 546–560, 2006.
Venterea, R. T., Spokas, K. A., and Baker, J. M.: Accuracy and Precision Analysis of Chamber-Based Nitrous Oxide Gas Flux Estimates, Soil Sci. Soc. Am. J., 73, 1087–1093, 12009.
Weier, K. L., Doran, J. W., Power, J. F., and Walters, D. T.: Denitrification and dinitrogen nitrous-oxide ratio as affected by soil-water, available carbon and nitrate, Soil Sci. Soc. America J., 57, 66–72, 1993.
Werner, C., Butterbach-Bahl, K., Haas, E., Hickler, T., and Kiese, R.: A global inventory of N_2O emissions from tropical rainforest soils using a detailed biogeochemical model, Global Biogeochem. Cy., 21, GB3010, doi:10.1029/2006GB002909, 2007a.
Werner, C., Kiese, R., and Butterbach-Bahl, K.: Soil-atmosphere exchange of N_2O, CH_4, and CO_2 and controlling environmental factors for tropical rain forest sites in western Kenya, J. Geophys. Res.-Atmos., 112, D03308, doi:10.1029/2006jd007388, 2007b.
Wessen, E., Soderstrom, M., Stenberg, M., Bru, D., Hellman, M., Welsh, A., Thomsen, F., Klemedtson, L., Philippot, L., and Hallin, S.: Spatial distribution of ammonia-oxidizing bacteria and archaea across a 44-hectare farm related to ecosystem functioning, Isme J., 5, 1213–1225, 2011.
WMO: The state of greenhouse gases in the atmosphere using global observations through 2008, in: Greenhouse Gas Bulletin, World Meteorological Organization, 4, 2009.
WRB: World reference base for soil resources, 2006, FAO, Rome, 62, 67–68, 2006.
Xiong, Z. Q., Freney, J. R., Mosier, A. R., Zhu, Z. L., Lee, Y., and Yagi, K.: Impacts of population growth, changing food preferences and agricultural practices on the nitrogen cycle in East Asia, Nutrient Cycling in Agroecosystems, 80, 189–198, 2008.
Zhang, W., Mo, J. M., Yu, G. R., Fang, Y. T., Li, D. J., Lu, X. K., and Wang, H.: Emissions of nitrous oxide from three tropical forests in Southern China in response to simulated nitrogen deposition, Plant Soil, 306, 221–236, 2008.
Zhou, G. Y., Guan, L. L., Wei, X. H., Tang, X. L., Liu, S. G., Liu, J. X., Zhang, D. Q., and Yan, J. H.: Factors influencing leaf litter decomposition: an intersite decomposition experiment across China, Plant Soil, 311, 61–72, 2008.

BGD
9, 14945–14980, 2012

Zhu J., Mulder J., Solheimslid S., Dörsch P.: Functional traits of denitrification in a subtropical forest catchment in China with high atmogenic N deposition. Soil Biol. Biochem., doi:10.1016/j.soilbio.2012.09.017, in press, 2012.

Zhu J., Mulder J., Bakken L., and Dörsch P.: The importance of denitrification in N_2O emission from N-saturated forests of SW China; results from in situ ^{15}N labeling experiments, Biogeochemistry, submitted, 2012.

BGD

9, 14945–14980, 2012

Table 1. Characteristics of top soil of individual plots on the hill slope (HS) and in the groundwater discharge zone (GDZ)

plot		Horizon/layer	pH (H_2O)	TOC	TN	C/N	BD[a]	NH_4^+ ex	NO_3^- ex	NH_4^+ sw	NO_3^- sw	IDR[b]	Ex situ potential of N_2O loss[b]
				mg g^{-1}			g cm^{-3}	μ g N g^{-1}	dw soil	mgN l^{-1}		nmol N_2O-N g^{-1} dw soil h^{-1}	nmol NO_3^- g^{-1} dw soil
HS	T1	O	3.96	226.1	8.7	26.1	–	49.6	37.9	–	–	8.4	523
		A	3.78	10.7	0.5	20.4	0.78	21.5	59.6	0.11	15.66	12.2	552
	T2	O	3.74	354.5	15.7	22.6	–	81.9	23.7	–	–	16.7	2336
		A	3.84	15.0	0.8	19.4	0.72	34.4	12.7	0.75	14.86	13.3	1056
	T3	O	4.07	220.2	9.9	22.2	–	85.9	35.7	–	–	40.4	1924
		A	4.13	12.1	0.6	19.1	0.73	59.6	20.1	0.15	13.33	31.4	1624
	T4	O	3.74	326.0	13.4	24.3	–	89.2	29.1	–	–	6.4	460
		A	3.76	14.3	0.7	20.6	0.47	32.1	13.0	0.07	13.51	16.3	1556
	T5	O	3.67	218.1	10.1	21.6	–	55.3	33.6	–	–	26.5	1706
		A	3.75	6.5	0.4	17.2	0.76	25.8	17.4	0.07	13.42	14.7	1394
	B1	O	3.99	234.9	11.1	21.1	–	83.0	25.6	–	–	40.8	1236
		A	4.02	6.05	0.3	17.6	0.42	23.3	6.6	0.17	13.85	11.3	1014
GDZ[a]	B2	0–20 cm	4.46	14.5	0.9	15.6	1.57	3.6	6.30	1.25	6.25	1.8	318
	B3		4.31	12.8	0.7	18.6	1.67	2.8	2.56	0.01	1.51	12.3	494
	B4		4.38	23.1	1.6	14.5	0.69	7.9	1.62	0.02	5.44	21.0	53
	B5		4.42	11.8	0.8	14.4	0.63	2.9	2.39	0.02	0.66	20.1	201
	B6		4.80	40.5	2.8	14.7	1.01	4.3	0.59	1.12	0.20	28.0	357

TOC: total organic carbon; TN: total nitrogen; C / N: ratio of TOC and TN; BD: bulk density; NH_4^+ ex and NO_3^- ex: average 2M KCl-extractable NH_4^+ and NO_3^-; NH_4^+ sw and NO_3^- sw: dissolved NH_4^+ and NO_3^- in soil water and groundwater in summer 2010 (11 May–26 September); IDR: instantaneous denitrification rate in anoxic soil slurries with ample NO_3^-; Ex situ potential of N_2O loss: nmol NO_3^- g^{-1} dw soil denitrified before maximum N_2O reduction to N_2 was observed in anoxic soil slurries with ample supply of NO_3^-.

[a] data from Sørbotten (2011) obtained using 100 cm^3 steel cylinders in three replicates for A horizon for each sampling plot.

[b] Data from Zhu et al. (2012).

BGD
9, 14945–14980, 2012

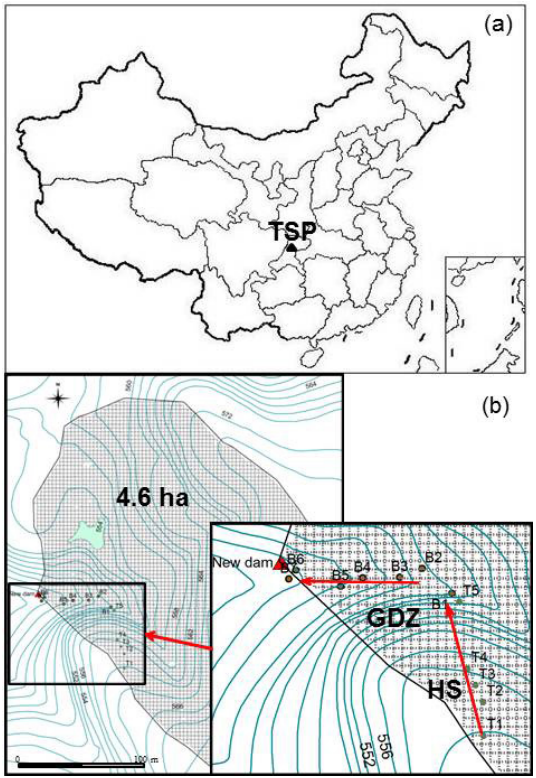

Fig. 1. Location of the Tieshanping (TSP) forest catchment, Chongqing, China **(a)** and plot layout in the TSP catchment **(b)**. Plots T1 to T5 constitute transect T on the hill slope (HS); plots B1 to B6 constitute transect B in the ground water discharge zone (GDZ). Increasing plot number denote decreasing elevation along the transects. Plots T5 and B1 are at the intersection of HS and GDZ.

BGD
9, 14945–14980, 2012

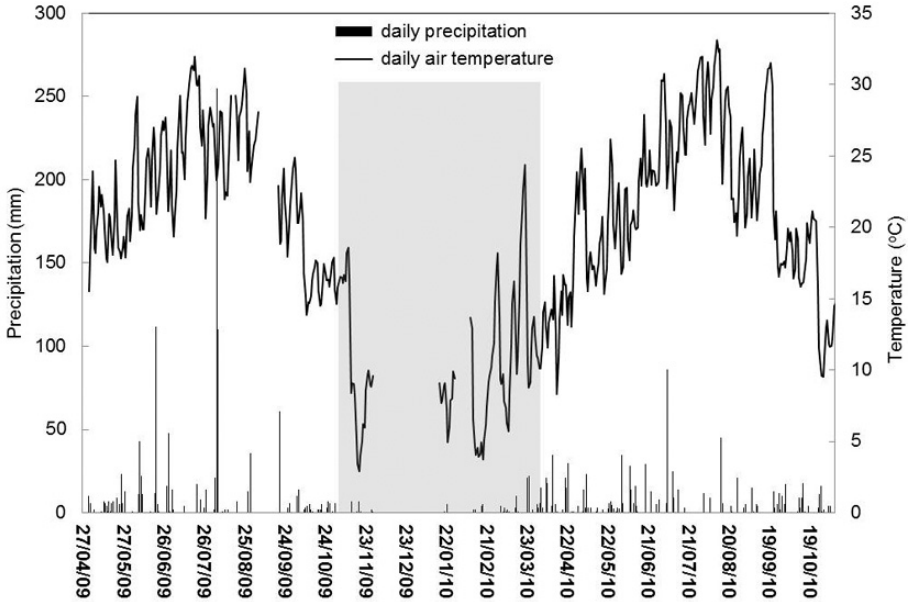

Fig. 2. Daily average air temperature and daily precipitation at TSP. The temperature data from 5 September to 18 September 2009, 29 November 2009 to 16 January 2010 and 29 January to 8 February 2010 were missing. Shaded area indicates the dry-cool season.

BGD
9, 14945–14980, 2012

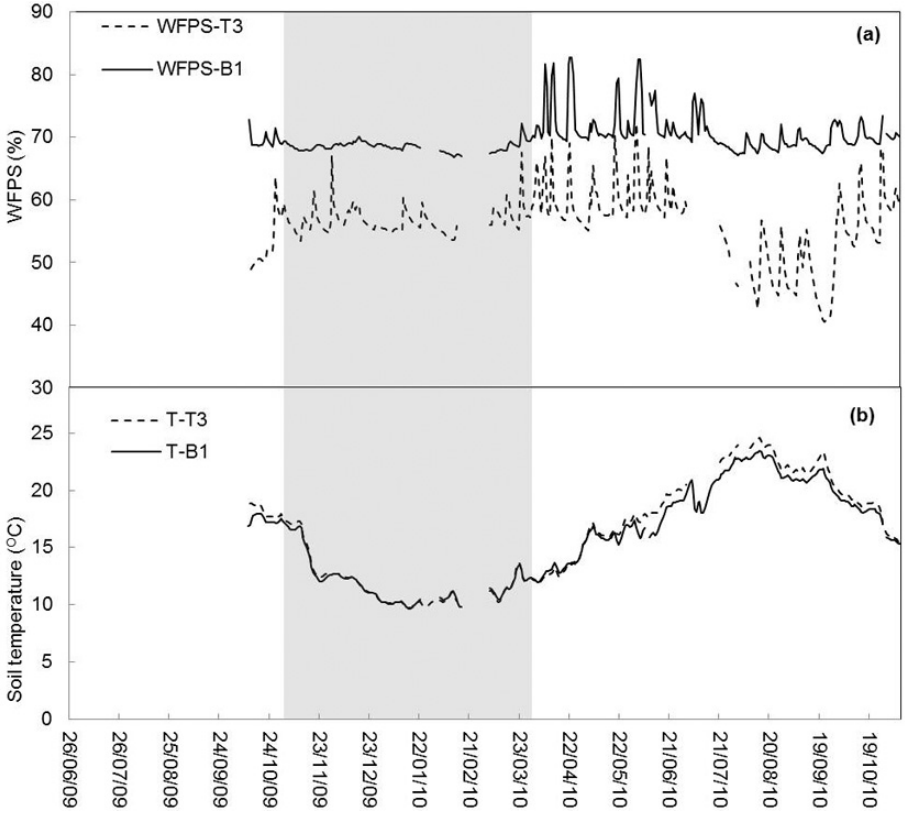

Fig. 3. Soil water filled pore space (WFPS, **a**) and soil temperature (ST, **b**) at 10 cm depth at plots T3 and B1. Shaded area indicates the dry-cool season.

BGD
9, 14945–14980, 2012

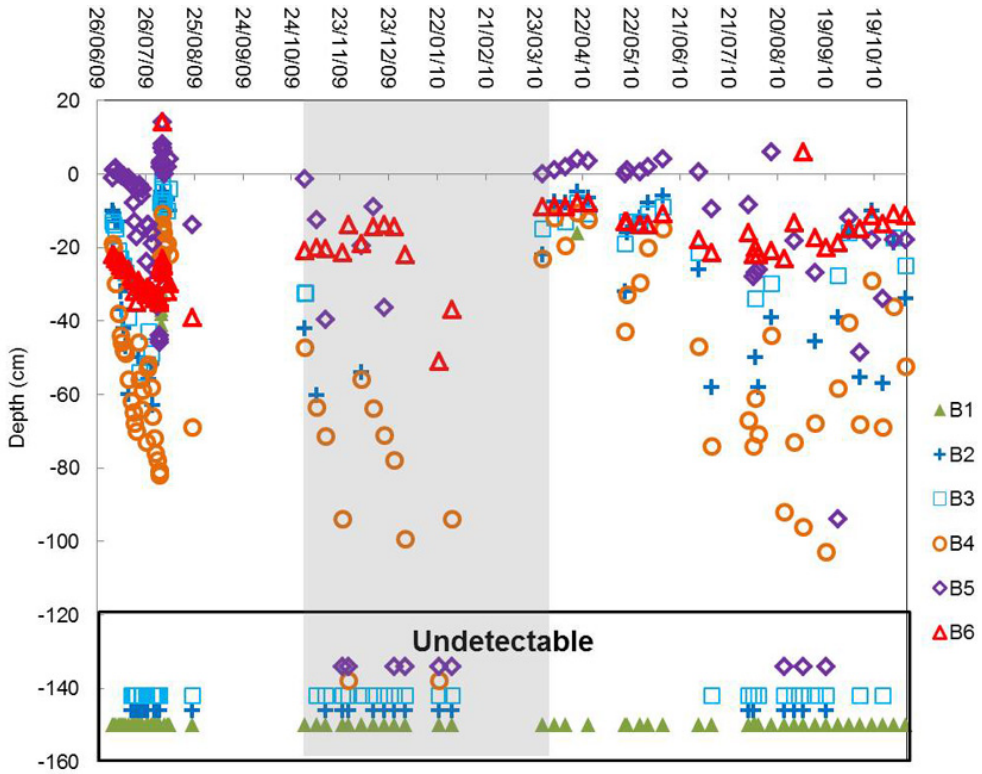

Fig. 4. Groundwater level (GWL) in GDZ. The lower panel indicates plots and dates at which the groundwater level was below the bottom of the monitoring well. Shaded area indicates the dry-cool season.

BGD
9, 14945–14980, 2012

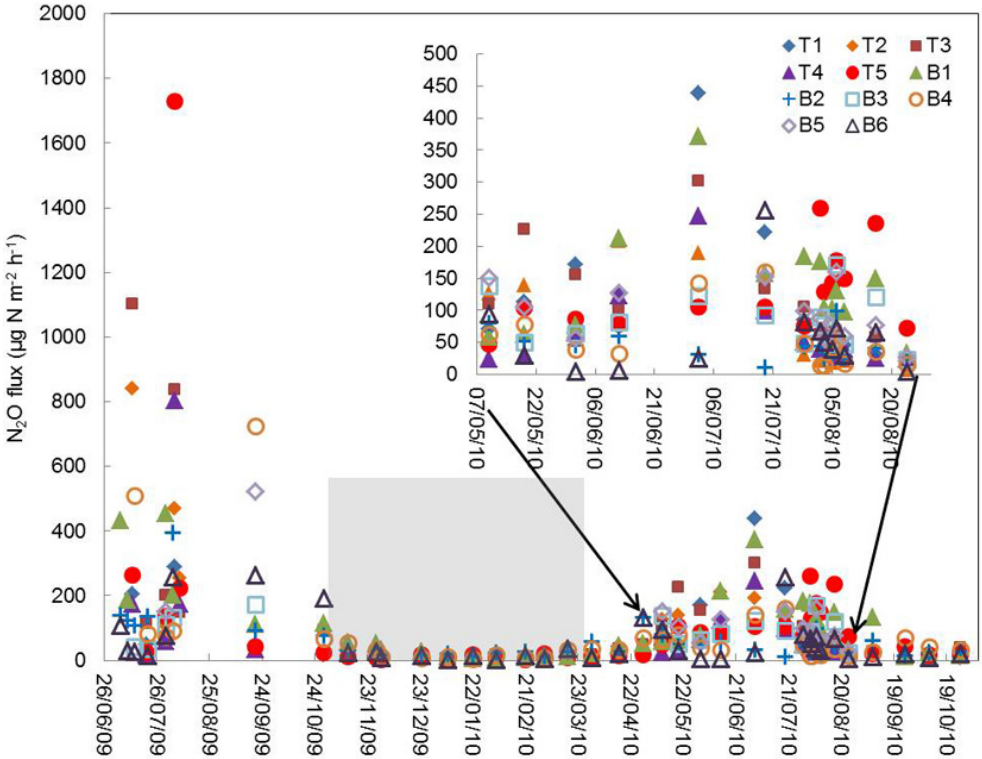

Fig. 5. Mean N_2O flux ($n = 3$) at the plots on the hill slope (HS) and in the ground water discharge zone (GDZ). Standard errors are not shown to maintain readability of the figure. Shaded area indicates the dry-cool season.

BGD
9, 14945–14980, 2012

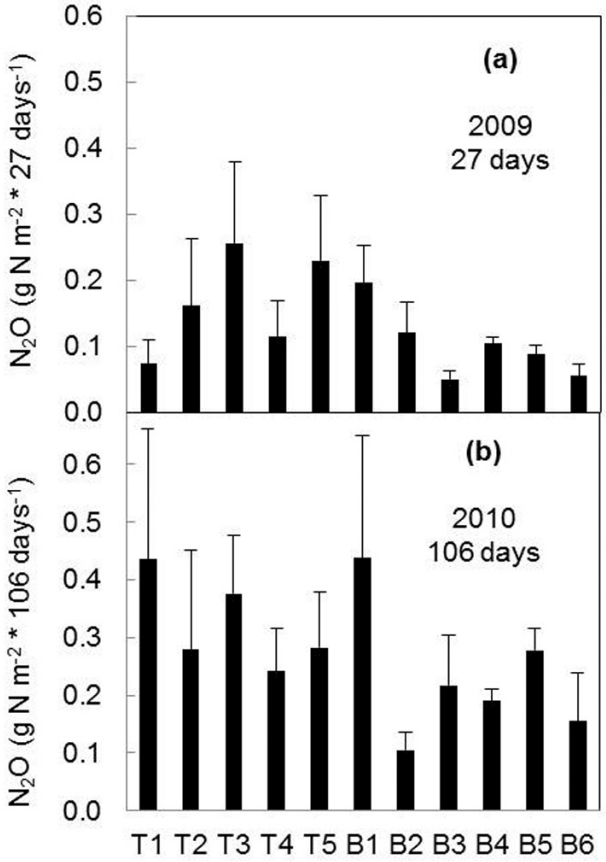

Fig. 6. Cumulative N_2O fluxes (g N_2O-N m^{-2}) during summer 2009 (**a**, from 12 July to 8 August, 27 days) and 2010 (**b**, from May 10 to 24 August, 106 days) at individual plots (n = 3). Error bars represent standard error.

BGD
9, 14945–14980, 2012

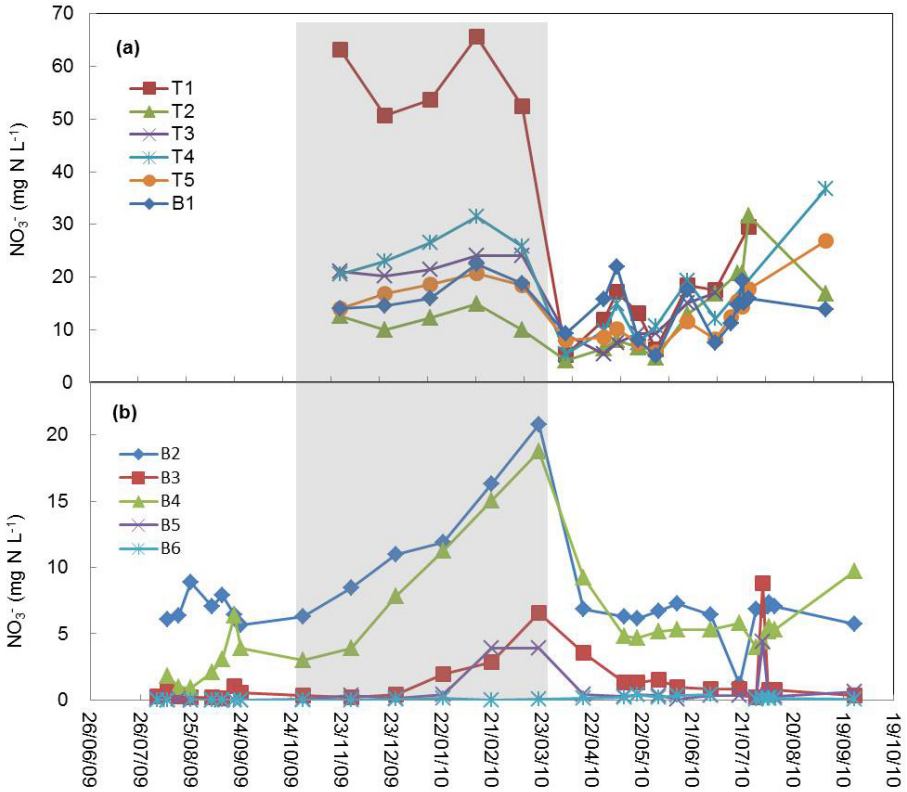

Fig. 7. NO_3^- concentration (mg N L^{-1}) in soil pore water at 5 cm depth at each plot of HS **(a)** and of groundwater at 30 cm depth in GDZ **(b)**, respectively. NO_3^- values from some of the HS plots during summer 2009 are missing because samplers were damaged by worms. Shaded area indicates the dry-cool season.

BGD
9, 14945–14980, 2012

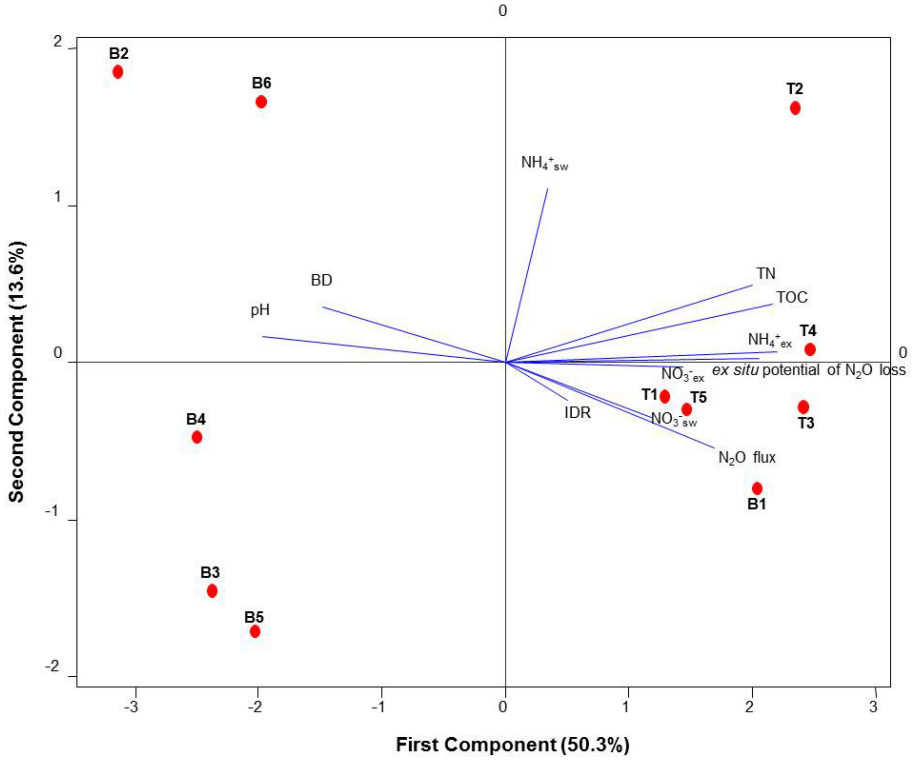

Fig. 8. Principal component analysis of cumulative N_2O fluxes and soil parameters (Table 1) at TSP. Before analysis, the N_2O flux and several of the parameters were transformed, whereas others (TOC: total organic carbon; TN: total nitrogen; C / N: the ratio of TOC and TN; IDR: instantaneous denitrification rate; ex situ potential of N_2O loss (see text for explanation); $NH_4^+{}_{ex}$ and $NO_3^-{}_{ex}$: 2M KCl -extractable NH_4^+ and NO_3^-) were not. The transformations were as follows: N_2O flux: ln (cumulative N_2O flux from each plot in summer 2010; Fig. 6); BD: −1/(bulk density); $NH_4^+{}_{sw}$: ln (dissolved NH_4^+) in soil water; $NO_3^-{}_{sw}$: sin(dissolved NO_3^- in soil water). Red points indicate the individual plots.

BGD
9, 14945–14980, 2012

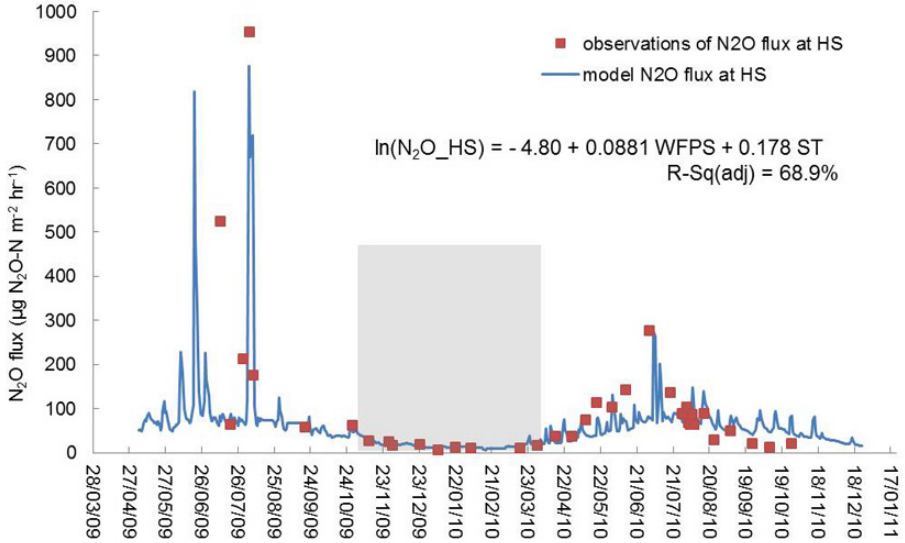

Fig. 9. Observed and simulated average N_2O flux at hill slope (HS). The shaded area denotes the dry-cool season.

BGD
9, 14945–14980, 2012